Article

Journal of Vibration and Control
1–13

DOI: 10.1177/1077546316644366
jvc.sagepub.com
SAGE

Simultaneous phase control of multiple frequencies of multi-degree-of-freedom systems

Tobias Brack[1], Robin Vujanic[2] and Jurg Dual[1]

Abstract

This paper presents an innovative method to achieve the simultaneous phase control of multiple resonance frequencies of a linear multi-degree-of-freedom system using only one sensor/actuator pair. Each frequency is manipulated independently by means of a PLL-based control loop which comprises a digital averaging phase detector that combines the two most crucial tasks, namely the phase shift measurement and the frequency separation. The properties of the controller are designed individually for each mode using a linearized model of the control system. The method is applicable to all kinds of oscillators where frequencies near the structure's natural frequencies are to be controlled. To validate the results experimentally, the controller is implemented on a digital signal processor (DSP) and applied to a torsional oscillator. Investigating two different damping conditions, the simultaneous control of five resonance frequencies of the oscillator illustrates the effectiveness and stability of the multiple frequency tracking. The method is able to significantly improve the accuracy and versatility of sensor applications. As an example a method is presented that enables the direct determination of the modal damping by using two frequencies corresponding to one single vibration mode.

Keywords

Vibration control, multi-mode vibrations, phase-locked loop, resonance tracking, damping measurement

1. Introduction

The eigenfrequencies and damping parameters of a linear oscillatory system are characteristic values that are dependent both on the system properties as well as on external influences. Therefore, using a control loop that enables a permanent excitation at resonance has led to the widespread principle of resonant sensors, which has become a common technique in research and in industry (e.g. Langdon, 1985). Since the resonance frequencies are altered by external influences, they can be related to the desired physical quantity by means of analytically or experimentally obtained relationships. Applications using this principle can be found in quartz crystal microbalances (Vives and Arnau, 2008), mass sensors (Kharrat et al., 2008) or DNA analysis chips (Rüst et al., 2013), amongst others. In the field of fluid characterization, frequency tracking using phase control provides an efficient approach for the development of on-line viscometers (Dual et al., 1990; Dual and O'Reilly, 1993; Häusler et al., 1996).

All these applications have in common that only one single frequency can be tracked at a time. However, in many applications the investigation of more values is required, for example to monitor frequency dependent behavior, to improve accuracy, or to compensate for possible errors. These tasks can be fulfilled by consecutively tracking multiple resonance frequencies of the oscillator (Stokich et al., 1994) or by simply using several independent oscillators as described by Blom and Mellema (1984). Both methods, though, show several disadvantages. The former case limits the application to the detection of slowly changing processes, since the

[1]Institute for Mechanical Systems, ETH Zurich, Switzerland
[2]Automatic Control Laboratory, ETH Zurich, Switzerland

Received: 7 May 2015; accepted: 19 March 2016

Corresponding author:
Tobias Brack, Institute for Mechanical Systems, ETH Zurich, Tannenstrasse 3 8092 Zurich, Switzerland.
Email: brack@imes.mavt.ethz.ch

consecutive tracking is time-consuming. The latter does not ensure the exact same condition is measured, e.g. due to different temperatures, cf. Vig (2001). Further the fabrication, calibration and operation of multiple sensors is more expensive.

It is therefore beneficial to track multiple resonance frequencies of a single oscillator at the same time. The simultaneous use of multiple resonance modes has been subject of research in the field of crystal oscillators. Vig (2001) described a method to minimize unwanted temperature-induced changes of the frequency of clock generators using a combination of two oscillation modes. Spurious parasitic capacitances are compensated in the same manner, which improves the performance of sensor applications (Arnau et al., 2008; Sell et al., 2011). However, since crystal oscillators maintain resonance oscillation by a simple feedback and amplification procedure, the techniques used in these applications do not support phase control and cannot easily be adapted to general oscillators.

This paper presents a novel control concept, which allows the simultaneous phase control of multiple resonance modes by using only one sensor/actuator pair. The method can be applied to all kinds of linear oscillators that exhibit several resonance frequencies, be it mechanical or electrical. This offers numerous possibilities for the improvement and enhancement of resonance based sensor principles, e.g. to measure both viscosity and density (Heinisch et al., 2014; Wattinger, 2014) or for rheological measurements (Brack and Dual, 2013).

The paper is structured as follows. First the fundamental principles of vibrations of continuous systems are reviewed. Next, the proposed control system structure is presented. It is based on the integration of the oscillator with a phase-locked loop (PLL) (e.g. Gökcek, 2003; Kutin et al., 2003; Park et al., 2009). Here, however, multiple PLL subsystems are used, each of them being responsible for the tracking of one specific frequency. Design rules are identified for synthesizing appropriate PI controllers for each subsystem. These results are first verified by numerical simulations that form the basis for the digital implementation of the necessary elements on a digital signal processor (DSP). The practical suitability of the method is then demonstrated on a torsional oscillator that is used in viscometry. Besides tracking multiple resonance frequencies, the experiments show that the method is also capable of simultaneously controlling two adjacent, nonresonant frequencies.

2. The oscillating system

In the following section the fundamentals of vibrations of continuous mechanical systems will be recalled. With regard to the system used for the experimental validation, we focus on the torsional dynamics of a homogeneous, circular rod with fixed-free boundary conditions, shown in Figure 1.

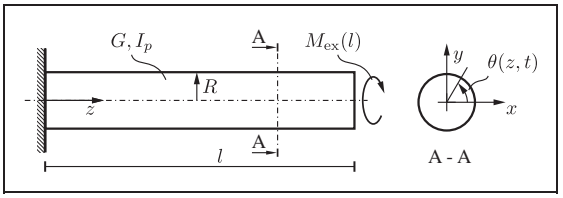

Figure 1. Simplified model of the torsional oscillator as a fixed-free circular rod of length l and radius R. The excitation moment is applied at the free end.

It is fixed at one end ($z = 0$) and excited by an external moment $M_{ex}(t)$ at $z = l$. The differential equation of motion is

$$\rho I_p \theta(z,t)_{,tt} - (G I_p \theta(z,t)_{,z})_{,z} = M_{ex}(t)\delta(z-l) \quad (1)$$

where $[\cdot]_{,z}$ represents the partial derivative with respect to the coordinate z, $[\cdot]_{,tt}$ indicates double partial differentiation with respect to time and δ is the Dirac delta function. The dependent variable $\theta(z, t)$ describes the angular displacement, I_p is the polar moment of inertia, ρ the density and G the (complex) shear modulus of the material. Internal material damping may be incorporated by including a viscous term in the expression of stress which constitutes the imaginary part of the complex shear modulus as described in Hagedorn and DasGupta (2007). Geometric and mechanical properties are assumed to be constant over the length of the rod. Taking the boundary conditions $\theta(0, t) = 0$ (fixed end, no movement) and $G I_p \theta_{,z}(l, t) = 0$ (free end, zero moment) into account, the homogeneous solution can be derived analytically up to an arbitrary constant C_m, yielding an infinite number of solutions indexed by m of the form

$$\theta_m(z,t) = C_m \sin\left(\frac{\omega_{0,m}}{c} z\right) e^{i\omega_{0,m} t} = W_m(z) e^{i\omega_{0,m} t} \quad (2)$$

The angular resonance frequencies[1] $\omega_{0,m}$ and the torsional wave speed c are defined by

$$\omega_{0,m} = \frac{c}{l}\left(m - \frac{1}{2}\right)\pi, \quad m = 1 \ldots \infty \quad (3)$$

$$c = \sqrt{\frac{G}{\rho}} \quad (4)$$

Unlike a single degree of freedom (dof) system, which is characterized by a single resonance frequency, the continuous system exhibits an infinite number of

resonance frequencies. Each resonance frequency is related to the mode shape $W_m(z)$ that describes a specific pattern of motion in which all parts of the system move with the related frequency. Based on the orthogonality of the mode shape functions it can be shown that any physically possible shape of the system can be represented by a linear combination of the mode shapes (Hagedorn and DasGupta, 2007).

Let us assume an excitation moment

$$M_{\mathrm{ex}}(t) = \sum_{n=1}^{k} M_n \sin(\omega_n t) \tag{5}$$

composed of multiple sinusoidal signals with amplitude M_n and frequency ω_n. Due to the superposition principle, this will lead to the steady state response of the angular velocity $\bar{\theta}_{,t}$

$$\bar{\theta}_{,t}(z_r, t) = \sum_{n=1}^{k} \left| Y(\omega_n) \right| M_n \sin(\omega_n t + \angle Y(\omega_n)) \tag{6}$$

measured at $z = z_r$. The function $Y(\omega)$ is known as the (complex) structural mobility function, usually represented by the amplification $|Y(\omega)|$ and phase shift $\angle Y(\omega)$ with respect to the excitation signal. Following the analysis in (Fahy and Gardonio, 2007), the mobility function can be represented by a summation of the modal contributions to the response of the system. If there is a significant difference between the resonance frequencies and the modal damping is small, the contribution of other modes can be neglected if the excitation frequency is near to a specific resonance frequency. In this range the mobility function can be approximated by the well-known equation of a linear single dof system, which yields the phase shift

$$\angle Y(\omega)|_{\omega \approx \omega_{0m}} \approx \arctan\left(\frac{\omega_{0,m}^2 - \omega^2}{2 D_m \omega_{0,m} \omega} \right) \tag{7}$$

where D_m describes the modal damping ratio. It is useful to express the damping ratio in terms of frequency difference $\Delta\omega_m$ of two frequencies corresponding to the phase values $\Delta\phi_{0,m} \pm \alpha$ via

$$D_m = \frac{\Delta\omega_m}{2\omega_{0,m} \tan(\alpha)} \tag{8}$$

3. Control loop design

3.1. PLL-based control loop for frequency tracking

Since every oscillator exhibits a particular relation between oscillation frequency and phase shift of the response with respect to the excitation, phase control is well suited to achieve the frequency tracking. This can be achieved by the use of a Phase-locked loop (PLL). Nowadays, PLL techniques are found in numerous application domains, such as communication technology (e.g Hsieh and Hung, 1996; Gardner, 2005) or mechatronics (Wang et al., 2007). The fundamental working principle of a PLL is the frequency adaption of a harmonic output signal to an external input based on the phase shift between both signals. Therefore, the frequency tracking of oscillators can be achieved by incorporating the oscillating system into the classical PLL scheme, as shown in Figure 2.

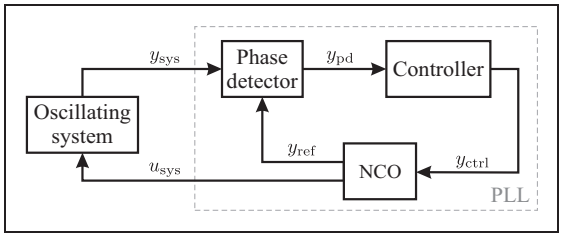

Figure 2. Block diagram of a PLL in conjunction with an oscillating system. The elements of the conventional PLL, i.e. phase detector, controller and numerically controlled oscillator (NCO), are framed by the dashed box.

In this control scheme, the numerically controlled oscillator (NCO) generates the excitation signal

$$u_{\mathrm{sys}}(t) = U_0 \sin(\phi_{\mathrm{nco}}(t)), \quad \phi_{\mathrm{nco}}(t) = \int_0^t \omega(\bar{t}) \mathrm{d}\bar{t} \tag{9}$$

with an amplitude U_0 that can be set freely. The frequency ω is dependent on the NCO input y_{ctrl} via

$$\omega(t) = \omega_c + K_{\mathrm{nco}} y_{\mathrm{ctrl}}(t) \tag{10}$$

where ω_c is called *center frequency* and K_{nco} is a constant gain factor with units of rad/s. The phase ϕ_{nco} is the integral over time of the (varying) excitation frequency ω

The oscillating system is assumed to be linear, hence it will respond to the excitation with a phase-shifted signal with different amplitude A_{sys} and phase difference $\Delta\phi_{\mathrm{sys}}$ sys

$$y_{\mathrm{sys}}(t) = A_{\mathrm{sys}}(t) \sin(\phi_{\mathrm{sys}}(t)) \tag{11a}$$

$$\phi_{\mathrm{sys}}(t) = \phi_{\mathrm{nco}}(t) + \Delta\phi_{\mathrm{sys}}(t) \tag{11b}$$

The phase detector extracts the difference between the phase of the response signal y_{sys} and the phase of a reference signal

$$y_{\mathrm{ref}}(t) = \sin(\phi_{\mathrm{ref}}(t)) \tag{12a}$$

$$\phi_{\mathrm{ref}}(t) = \phi_{\mathrm{nco}}(t) + \Delta\phi_{\mathrm{ref}} \tag{12b}$$

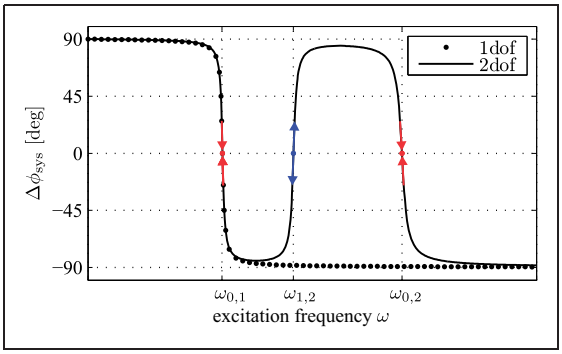

Figure 3. Qualitative illustration of the phase of the mobility function of a linear oscillator with both one (dotted line) and two (solid line) degrees of freedom. The colored points illustrate the stable (red) and unstable (blue) equilibrium points for positive controller gain and. $\Delta\phi_{\text{ref}} = 0$. The arrows illustrate the attraction (red) and repulsion (blue) of the excitation frequency.

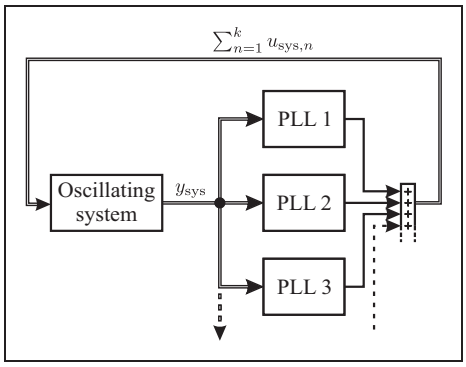

Figure 4. Illustration of the multi-frequency control loop comprising a parallel arrangement of multiple PLL subsystems, an adder and the oscillating system. A single line represents a harmonic signal containing a single frequency, a double line represents a multi-frequency signal.

that implies an additional phase shift $\Delta\phi_{\text{ref}}$. Hence, the output of the phase detector yields

$$y_{\text{pd}}(t) = \phi_{\text{sys}}(t) - \phi_{\text{ref}}(t) = \Delta\phi_{\text{sys}}(t) - \Delta\phi_{\text{ref}} \qquad (13)$$

To close the loop, the phase difference y_{pd} is used as control error of the controller whose output y_{ctrl} is connected to the NCO. Consequently, a positive controller increases the frequency and vice-versa. Since damping causes transient effects of the oscillator to decay, the equilibrium value of the phase shift $\Delta\phi_{\text{sys}}$ is the steady state value.

If the oscillating system is a linear, 1dof system, the steady state relationship between excitation frequency and phase shift is described by equation (7). As depicted in Figure 3 (dotted line), the phase shift has a continuous negative gradient; hence, the control error converges to zero if the controller has positive gain and at least one integral term (Sun et al., 2002; Brack et al., 2015). Therefore, the excitation frequency ω will settle down at the frequency that corresponds to the steady state phase shift between excitation (input u_{sys}) and response (output y_{sys}) that is given by $\Delta\phi_{\text{ref}}$.

If the oscillating system exhibits several resonance frequencies, however, the relation between frequency and phase shift is no longer unique. As an example, Figure 3 shows the phase of the mobility function of a 2dof, where zero phase shift can be found at the resonance frequencies $\omega_{0,1}$ and $\omega_{0,2}$ (red dots) and at the anti-resonance frequency $\omega_{1,2}$ (blue dot). Still having positive controller gain, the frequency tracking works analog to the 1dof situation A positive phase shift increases the excitation frequency and vice versa, so only the frequencies around resonance are stable equilibrium points, whereas the frequencies around the anti-resonance represent unstable equilibrium points, as illustrated in the figure for $\Delta\phi_{\text{ref}} = 0$. This leads to the identification of an attraction region for a specific mode that is defined by the adjacent anti-resonance frequencies (Kern et al., 2012).

3.2. Multiple frequency tracking

As described before, the excitation of a linear oscillator with a harmonic, multi-frequency signal causes a system response that can be regarded as a superposition of the responses to the corresponding single frequency excitations. Therefore, a parallel arrangement of k PLL subsystems can be used for the simultaneous tracking of multiple frequencies, as illustrated in Figure 4. Each PLL is responsible for the phase control of one single frequency that is generated by the corresponding NCO. The output signals are added together and form the excitation signal of the system. Consequently, the input signal of each PLL is composed of multiple frequencies, hence an effective extraction of the specific frequency is of utmost importance. This could be achieved for example by using narrow band-pass filters, as presented by Tjahyadi et al. (2006). Discrete Fourier transform methods could also be applied, notably using the Goertzel algorithm which evaluates amplitude and phase at a single selectable frequency, (cf. Oppenheim et al., 1999). (Sell et al., 2011) used this method for the compensation of spurious parallel capacitances of piezoelectric sensors. Another possibility is described in the work of (Clarke, 2002), who used the Hilbert transform phase detector (HTPSD) to process signals with high signal to noise ratio. However, these methods impose different restrictions on the application. Leakage errors can occur when dealing with DFT algorithms, while both the HTPSD and band-pass methods require filters of a very high order to obtain accurate results.

Using a digital averaging phase detector (APD), the frequency separation can be combined with the phase

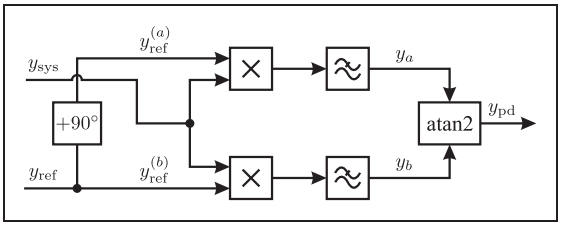

Figure 5. Block diagram of the digital averaging phase detector. The output y_{pd} corresponds to the phase difference between the input signals y_{sys} and y_{ref}. The symbol $\times$ denotes a multiplier, $\approx$ symbolizes a low-pass filter.

detection in a single element that is composed of simple elements and does not possess the problems of the aforementioned methods. Figure 5 shows the structure of the APD as it is implemented in various applications, especially in digital lock-in amplifiers (Gaspar et al., 2004).

To explain the functionality of the APD, steady state is assumed, i.e. transient vibrations have diminished. As with equation (6), the output of the oscillator can be written as a sum of k harmonics

$$y_{\text{sys}}(t) = \sum_{n=1}^{k} A_n \sin(\omega_n t + \Delta\phi_n) \tag{14}$$

As a generic example, the first PLL (PLL1) that is responsible for the phase control of the excitation frequency ω_1 is now studied more closely. According to Figure 5, the reference signal is phase shifted by 90 degrees to obtain two parts

$$y_{\text{ref},1}^{(a)}(t) = \cos\big(\omega_1 t + \Delta\phi_{\text{ref},1}\big) \tag{15a}$$

$$y_{\text{ref},1}^{(b)}(t) = \sin\big(\omega_1 t + \Delta\phi_{\text{ref},1}\big) \tag{15b}$$

that are both multiplied by the system response, which gives

$$y_{\text{ref},1}^{(a)} \cdot y_{\text{sys}} = \sum_{n=1}^{k} \left[A_n \frac{1}{2} \big(\sin\big((\omega_n - \omega_1)t + \Delta\phi_n - \Delta\phi_{\text{ref},1}\big) + \sin\big((\omega_n + \omega_1)t + \Delta\phi_n + \Delta\phi_{\text{ref},1}\big)\big) \right] \tag{16a}$$

$$y_{\text{ref},1}^{(b)} \cdot y_{\text{sys}} = \sum_{n=1}^{k} \left[A_n \frac{1}{2} \big(\cos\big((\omega_n - \omega_1)t + \Delta\phi_n - \Delta\phi_{\text{ref},1}\big) - \cos\big((\omega_n + \omega_1)t + \Delta\phi_n + \Delta\phi_{\text{ref},1}\big)\big) \right] \tag{16b}$$

If there is a significant difference between the frequencies of the PLLs, all components except the DC value can be attenuated by using a low-pass filter with a cut-off frequency significantly below the smallest frequency difference (i.e. $\omega_2 - \omega_1$). Hence the filtered signals y_a and y_b can be approximated by

$$y_{a,1} \approx A_1 \frac{1}{2} \sin(\Delta\phi_1 - \Delta\phi_{\text{ref},1}) \tag{17a}$$

$$y_{b,1} \approx A_1 \frac{1}{2} \cos(\Delta\phi_1 - \Delta\phi_{\text{ref},1}) \tag{17b}$$

They can be regarded as real and imaginary parts of a complex number having the amplitude $A_1/2$ and argument $\Delta\phi_1$. Using the atan2 function, the phase shift

$$y_{\text{pd},1} = \text{atan2}(y_{a,1}, y_{b,1}) = \Delta\phi_1 - \Delta\phi_{\text{ref},1} \tag{18}$$

corresponding to the frequency ω_1 can be extracted. The amplitude A_1 is given by

$$A_1 = 2\sqrt{y_{a,1}^2 + y_{b,1}^2} \tag{19}$$

3.3. Synthesis of the control

In contrast to the conventional PLL, the combination of a PLL and an oscillator forms a nonlinear system due to the conversion of sinusoidal signals to nonharmonic phase signals. To be able to design the controller of each subsystem, a linearized model of the closed loop system is necessary.

We start with an analysis in which interactions between the PLL subsystems are neglected and one single system is regarded. Since each system can be modelled identically the index n will be omitted.

In order to enable a dynamic analysis of the control loop, a description of all elements in the Laplace domain is sought[2]. It is convenient to describe all input and output signals in terms of phase or frequency signals, which directly yields the description of the elements of the conventional PLL as linear, time-invariant systems. Further analysis is only necessary to describe the dynamic behavior of the oscillating system. In Laplace domain, the NCO is described by

$$\Omega(s) = \omega_c + K_{\text{nco}}\, Y_{\text{ctrl}}(s) \tag{20}$$

analog to equation (10). Next, the phase detector has to be described. (Brack et al., 2015) argued that its dynamic behavior is influenced mainly by the low-pass filter. In this analysis the filter is realized as a second order Butterworth filter, characterized by the

cut-off frequency $\omega_{3\mathrm{dB}}$. Hence the phase detector can be described in the Laplace domain by

$$Y_{\mathrm{pd}}(s) = (\Delta\Phi_{\mathrm{sys}} - \Delta\Phi_{\mathrm{ref}}) \cdot H_{\mathrm{LP}}(s) \tag{21}$$

$$H_{\mathrm{LP}}(s) = \frac{\omega_{3\mathrm{dB}}^2}{s^2 + \sqrt{2}\omega_{3\mathrm{dB}}s + \omega_{3\mathrm{dB}}^2} \tag{22}$$

Furthermore, the dynamic behavior of the phase shift $\Delta\Phi_{\mathrm{sys}}$ of the oscillator, with respect to a changing excitation frequency, is required. However, the phase-frequency relationship defined by the mobility function cannot be used for dynamic analysis, since it considers the steady state only. To overcome this, we use the modeling of phase dynamics introduced in (Brack et al., 2015). According to their work, the phase dynamics is approximated by a first order system linearized around the corresponding resonance frequency. This model is suitable as well for our continuous system due to the 1dof approximation around resonance. The equations describing the phase dynamics are given by

$$\Delta\Phi_{\mathrm{sys}}(s) = -H_{\mathrm{sys},m}(s)(\Omega(s) - \omega_{0,m}) \tag{23}$$

$$H_{\mathrm{sys},m}(s) = \frac{1}{D_m\omega_{0,m} + s} \tag{24}$$

The control loop is now completely described by the introduced linear systems and can be represented in the form of a classical feedback loop, as shown in Figure 6. Additionally, a disturbance signal S has been added. Choosing the center frequency equal to the resonance frequency, we obtain the following closed loop transfer function

$$H_{\mathrm{CL}}(s) = \frac{\Delta\Phi_{\mathrm{sys}}}{\Delta\Phi_{\mathrm{ref}}} = \frac{H_{\mathrm{LP}}H_{\mathrm{ctrl}}K_{\mathrm{nco}}H_{\mathrm{sys},m}}{1 + H_{\mathrm{LP}}H_{\mathrm{ctrl}}K_{\mathrm{nco}}H_{\mathrm{sys},m}} \tag{25}$$

for $S = 0$. To design the dynamic behavior of the system a PI controller is chosen, since it shows a high degree of robustness in the experiments and has the advantage of having very modest computational requirements, which is crucial for its implementation on a real-time embedded platform. The transfer function of a PI controller is given by

$$H_{\mathrm{ctrl}}(s) = K_P\frac{T_I s + 1}{T_I s} \tag{26}$$

with the proportional gain K_P and integral time constant T_I. From equation (25), the plant of the closed loop system is identified as

$$H_{\mathrm{plant}}(s) = H_{\mathrm{LP}}K_{\mathrm{nco}}H_{\mathrm{sys},m} \tag{27}$$

that shows no zero and three poles

$$p_1 = -D_m\omega_{0,m} \tag{28}$$

$$p_{2,3} = \frac{1}{\sqrt{2}}(-1 \pm \mathrm{i})\omega_{3\mathrm{dB}} \tag{29}$$

where only the pole p_1 is dependent on the properties of the oscillating system. To achieve a similar closed loop dynamics of all modes, the zero of the PI controller is set equal to p_1 by defining

$$T_I = \frac{1}{D_m\omega_{0,m}} \tag{30}$$

such that pole p_1 cancels out and the resulting transfer function is only dependent on the constant parameters K_{nco}, K_P and $\omega_{3\mathrm{dB}}$. Assuming $\omega_{3\mathrm{dB}} \gg 1$ rad/s, the closed loop transfer function can be approximated by

$$H_{\mathrm{CL}}(s) \approx \frac{K_{\mathrm{nco}}K_P}{K_{\mathrm{nco}}K_P + s} \tag{31}$$

which is a first order element with gain one and the time constant $T_c = 1/(K_{\mathrm{nco}}K_P)$. Thus we can specify the dynamic behavior of the closed loop system by choosing the appropriate parameters, given that the properties of the oscillating system are known. To obtain the dynamic behavior of the frequency, which is the major output of the phase control, the phase transfer function (25) has to be multiplied by $1/H_{\mathrm{sys},m}$, as can be deduced from Figure 6. This adds an additional zero to the closed loop transfer function, which does not change the time constant but creates a certain overshoot that is dependent on the modal damping ratio. Note that this result is only valid around a resonance frequency $\omega_{0,m}$, due to the linearization of the phase dynamics. If the system properties are not known exactly, pole p_1 will not be perfectly eliminated and the dynamic behavior will differ slightly from the prediction. However, since p_1 is a stable pole, these uncertainties will not cause

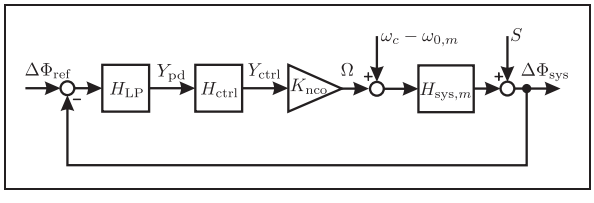

Figure 6. Linearized model of a PLL subsystem. The oscillating system is represented by the linearized phase dynamics of a linear first order system. The index *n* is omitted in the figure.

problems in terms of stability. Hence, the linearized system is stable for all positive parameters K_P, T_I and K_{nco}, which proves the nonlinear system to be stable around the resonance as well. The stability region is beyond the scope of this paper, the interested reader is referred to Brack et al. (2015).

Up to now, each subsystem has been regarded as independent of the others. During multi-frequency control, however, interactions between the subsystems might lead to effects that have not been considered yet. We model these interactions as an additive disturbance S on the measured signal of the phase, cf. Figure 6. According to equations (16)–(17), this disturbance is the AC component in the phase detector output Y_{PD} that remains after low-pass filtering. Hence, the disturbance contains the (relative) frequencies of all other subsystems.

Using the PI controller with the previously defined parameters, the disturbance transfer functions can be approximated by

$$\frac{\Delta\Phi_{\mathrm{sys}}}{S} \approx \frac{T_c s}{T_c s + 1} \tag{32}$$

$$\frac{\Omega}{S} \approx \frac{\sqrt{2}T_c s^2 + T_c s\omega_{3\mathrm{dB}} + \omega_{3\mathrm{dB}}}{(D_m\omega_{0,m} + s)\omega_{3\mathrm{dB}}} \tag{33}$$

for $\Delta\Phi_{\mathrm{ref}} = 0$ and $\omega_{3\mathrm{dB}} \gg 1$ rad/s. Both transfer functions show only stable poles, so closed-loop stability is still ensured for each subsystem. Since the disturbance will be transferred to the frequency output, the frequencies of the oscillation will vary slightly. This will not, however, change the amplitude of the disturbance but add an additional high-frequency component, cf. equation (16). Additionally, equation (33) exhibits low-pass behavior, so the disturbance will be additionally attenuated in the frequency output. Thus it can be stated that the parallel arrangement of multiple PLL systems will have no negative effect on the stability of each subsystem.

4. Validation

4.1. Experimental setup

To investigate the practical suitability of the method, the control loop is implemented on a TMS320C6747 floating point digital signal processor (DSP) from Texas Instruments with a closed-loop sampling frequency of 48 kHz. A torsional oscillator, originally used for viscosity measurements (Dual et al., 1990), serves as oscillating system. The excitation moment is applied electromagnetically using a coil system, a voltage-to-current converter is used to maintain a frequency independent excitation amplitude. A single-point laser vibrometer (Polytec OFV 303 sensor head with OFV 3001 controller) detects the system response in the form of angular velocity by eccentric measurement. The setup is shown in Figure 7.

First, the properties of the oscillating system were examined. To study the effect of possible interaction between the modes, two different damping conditions were created by using the oscillator vibrating freely in air and damped by a liquid. A highly viscous Newtonian calibration oil with a dynamic viscosity of 2.5 Pa s at 22°C serves as a damping liquid.

Using the control loop described in the previous section in open-loop mode, the mobility function for the ratio between the complex amplitudes of the angular velocity and the excitation voltage can be determined experimentally. Figure 8 shows the mobility function for both conditions in the frequency range of 0 to 20 kHz. In this frequency range the first five torsional resonance frequencies of the sensor can be clearly identified by a local amplitude maximum and a drop of the phase by −180 degrees. The anti-resonances are identified analogously and marked in the figure to visualize the attraction region for each resonance mode. As described by (Dual and O'Reilly, 1993), an increase of the damping and a decrease of the resonance frequencies of the torsional modes due to the fluid can be observed. The small amplitude peaks and phase drops at 1520 Hz, 3500 Hz, 7920 Hz, 12660 Hz and 18140 Hz correspond to flexural resonances of the oscillator (confirmed by FEM Simulations), indicating that the electromagnetic excitation is not purely torsional.

The measurement indicates that the APD is able to measure the phase shift over the whole frequency range. Therefore, the center frequencies can be freely chosen

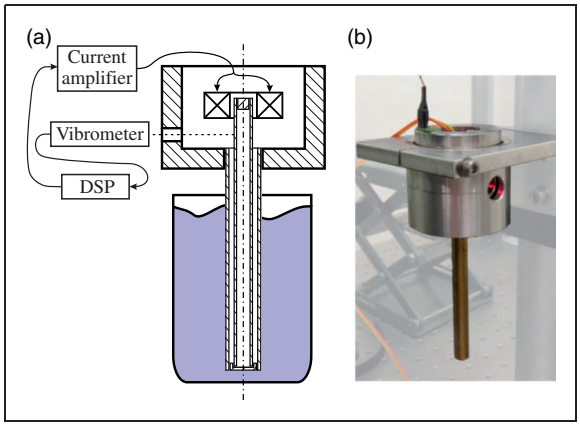

Figure 7. Experimental setup for the validation of the multi-frequency control method: (a) schematic illustration of the setup, including a section view of the oscillator; (b) photo of the torsional oscillator.

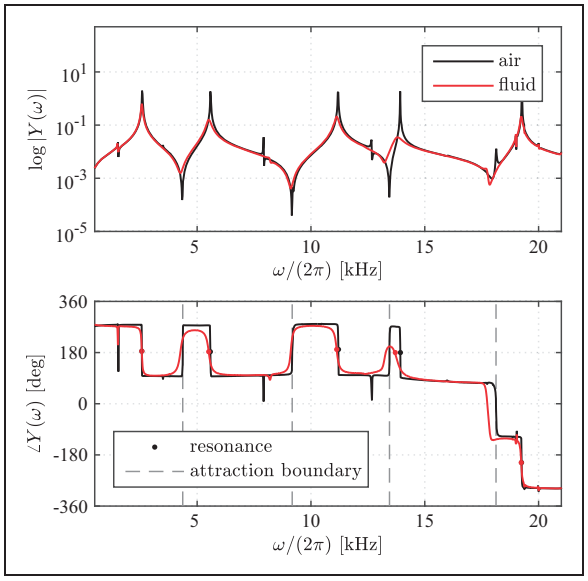

Figure 8. Amplitude (logarithmic scale) and phase of the mobility function of the torsional oscillator for both damping conditions, measured experimentally in open-loop mode. The vertical dashed lines correspond to the anti-resonances that define the attraction regions of each resonance mode, marked by black and red dots.

Table 1. Resonance frequencies and modal damping ratios of the first five torsional modes of the oscillator in air and damped by a fluid, measured independently for each mode.

	$\omega_{0,m}/(2\pi)$ (Hz)		D_m (10^{-3})	
Mode number m	Air	Fluid	Air	Fluid
1	2589.2	2569.6	0.043	9.59
2	5588.9	5508.9	0.05	16.66
3	11191.2	11130.2	0.099	6.46
4	13919.8	13774.1	0.073	12.69
5	19270.2	19240.6	0.155	1.71

within the appropriate attraction region to achieve successful resonance tracking.

While the assumption of separated modes is mostly valid for both conditions, the mobility function of the damped oscillator shows interactions between the third and fourth mode. The impact of this interaction on the simultaneous control will be discussed later. Based on the modal decomposition approach, the resonance frequencies and damping factors of each mode can be evaluated by fitting the 1dof equation (6) to the phase of the mobility function around the resonance values[3]. The obtained values are summarized in Table 1. The phase shift values at resonance, which are independent of the damping as long as the interaction between the modes is negligible, are indicated in Figure 8 by black and red dots, respectively. Due to parasitic phase shifts in the additional elements (e.g. excitation coil, laser, etc.), the resonance and anti-resonance frequencies do not show a phase shift of zero or a multiple of 360 degrees.

Two experiments have been performed to study the presented method: first, the simultaneous tracking of the first five resonance frequencies is investigated for both damping situations. Since the control method is based on the frequency separation, the APD is the most important but also most critical element of the control loop. To investigate the capabilities of the method in terms of frequency selectivity, two nonresonant frequencies corresponding to the same mode are tracked simultaneously in a second experiment. This application is referred to as *direct damping measurement*, since it is useful to directly determine the damping of the specific mode.

Additionally, we report the results of MATLAB Simulink simulations, used for the design of the control scheme, and use them for comparison with the real physical measurements. To ensure best correspondence to the results generated by the DSP, a fixed-step discrete solver is selected, using the same sampling frequency of 48 kHz. The oscillating system is represented by a parallel connection of five linear second order systems, each having the previously specified properties. The discrete transfer functions are generated using the bilinear z-transformation as described by Oppenheim et al. (1999).

4.2. Results: resonance tracking

To track the first five resonance frequencies, five PLL subsystems are used, one for each resonance frequency. For all experiments, if not otherwise stated, a second order Butterworth low-pass filter with cut-off frequency $\omega_{3\,\mathrm{dB}} = 63$ rad/s is chosen for each PLL. This is sufficient to effectively attenuate all unwanted frequency components. Using the definitions from equations (30) and (31), and including the appropriate system parameters from Table 1, the controller parameters are calculated individually for each PLL so that the time constant of all subsystems is $T_{c,n} = 1$ sec. The NCO gain is set to $K_{\mathrm{nco}} = 1$ rad/s and the reference phase shifts are adjusted to the values received by the 1dof fitting of the lightly damped situation, cf. Figure 8.

We first investigate the effect of the attraction region on the tracking performance. For this, all center frequencies $\omega_{c,n}$ are set to 95% of the resonance values. The experiments are conducted with air as the surrounding medium. Figure 9 shows the evolution of the frequencies. Almost all excitation modes track resonance, demonstrating that the method works even

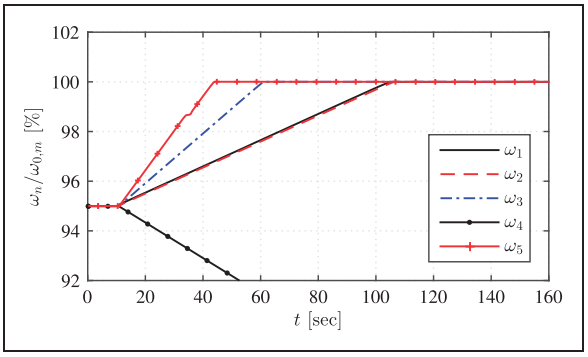

Figure 9. Evolution of the NCO frequencies ω_n relative to the resonance frequencies $\omega_{0,m}$ in air during the resonance tracking. Center frequencies are set to 95% of the resonance value. The control starts at $t = 10$ sec.

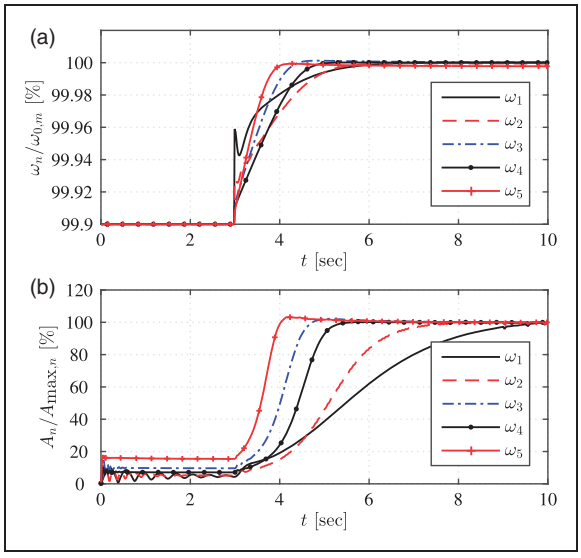

Figure 10. Evolution of the NCO frequencies ω_n relative to the resonance frequencies $\omega_{0,m}$ and normalized amplitudes of the torsional oscillator in air during the resonance tracking. Center frequencies are set to 99.9% of the resonance value. The control starts at $t = 3$ sec. (a) relative excitation frequencies, (b) normalized amplitudes.

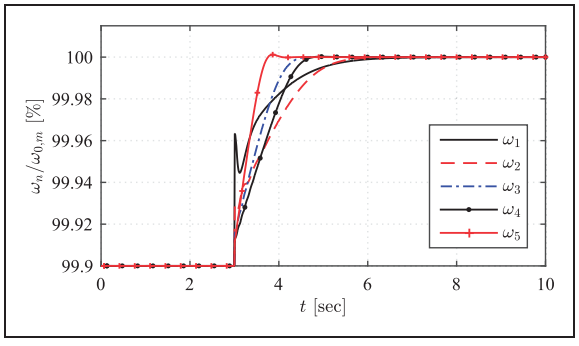

Figure 11. Evolution of the NCO frequencies ω_n relative to the resonance frequencies $\omega_{0,m}$ in air during the resonance tracking. Simulation result.

under conditions when the initial frequency is far from the corresponding resonance (and so even when the signal to noise ratio is bad). PLL 4, however, decreases its frequency. This is reasonable, since the center frequency $\omega_{c,4}$ is smaller than the anti-resonance $\omega_{3,4}$. Hence, in this case, the center frequency does not lie in the correct attraction region and ω_4 tracks to $\omega_{0,3}$. The simulations yield identical results which are therefore not shown in the figure.

Far from resonance, the phase dynamics of the oscillator is negligible. Hence, the coupling introduced by the phase dynamics can be neglected and the closed-loop dynamics of the controlled system can be considered independent. The controller design, however, is based on pole compensation, which generates different controller parameters and thus different closed-loop dynamics of the modes. The mode with the highest damping (mode 5) has the fastest controller and reaches resonance first, while modes 1 and 2 (the lowest damping ratios) are the last.

Next the dynamic behavior of the resonance tracking is investigated. Accordingly, the frequencies are set to start in or near to the region where the linearization is valid. More specifically, they are set to 99.9% of the resonance values for the lightly damped oscillator and to 99% for the damped situation. After three seconds the system is assumed to be in steady state and the control process is started by switching the controller parameters from zero to the specified values. The frequencies are then expected to approach the resonance frequencies within a period of about one second.

Figure 10 depicts the experimental results obtained for the freely vibrating oscillator. The final frequencies are reached after about two seconds with good accuracy. The dynamic behavior is still not exactly as aimed by the controller design, due to the very narrow frequency band in which the linearization is valid. Hence the different damping ratios of the modes are not entirely compensated by the controller, resulting in slightly different dynamics of each mode, similar to Figure 9. A small overshoot can be observed at the beginning of the control process which is caused by the non-continuous change from the starting value to the first value at $t = 3$ sec due to the digital characteristic of the control loop. Since the overshoot is dependent on the time constant of the oscillating system, it is mainly present at mode 1, cf. equation (24). As a comparison, the frequency tracking result obtained by simulations is shown in Figure 11. The conformity is very good, which reveals the Simulink model to be an effective approach to design and investigate the real system.

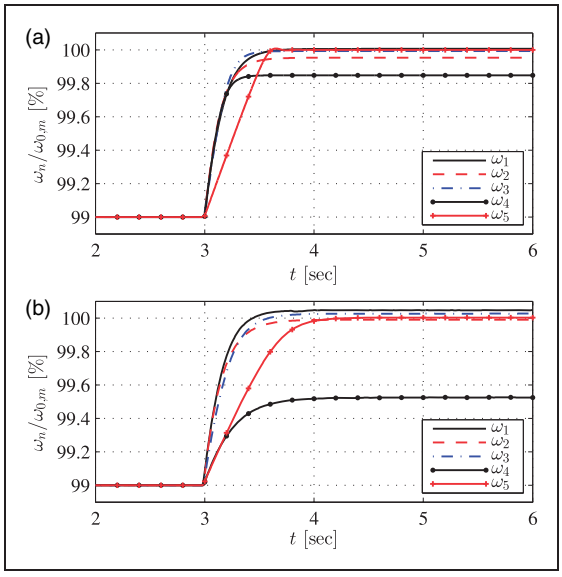

Figure 12. Evolution of the relative excitation frequencies of the fluid-damped torsional oscillator – (a) simulation result; (b) experimental result.

Figure 12 shows the simultaneous resonance tracking if the oscillator is damped by the fluid. Here the relative excitation frequencies obtained both from simulation and experiment are depicted. They evolve to the value specified in Table 1 with only small error. However, mode four settles down to 99.8% and 99.5% respectively of the resonance frequency. This error is caused by the non-negligible interaction of modes three and four. As can be seen by the location of the anti-resonance in air, mode four is more likely to be influenced by mode three than vice-versa. Hence, in the damped situation the phase around $\omega_{0,\ 4}$ cannot be approximated by the 1dof relationship from equation (7), which makes a unique identification of the resonance frequency impossible. Therefore, using the reference phase received from the measurement in air, the excitation frequency settles down at a frequency slightly different to the resonance value.

The design of the controller proves to be very effective for the investigated range of frequencies. The frequency evolution equals to the step response of a first order lag element, only the relatively low damped mode five deviates slightly from the predicted behavior for the same reason as in the lightly damped case.

4.3. Results: direct damping measurement

The determination of the damping is an important issue in many applications, for example in the field of viscometry. Equation (8) states that the knowledge of two frequencies corresponding to the phase values $\pm\alpha$ around the resonance phase shift is necessary to calculate the (modal) damping ratio of a specific mode. These two values are usually evaluated one after another by consecutively changing the reference phase. Using the presented method it is possible to measure the damping ratio without switching the reference phase by controlling the two required frequencies simultaneously. Thereby time is saved and measurement values are obtained at a much higher rate. In contrast to the simultaneous resonance tracking, the frequencies that have to be processed correspond in this case to the same vibration mode. Hence, depending on the resonance frequency and damping ratio of the investigated mode, they will be very close together, which puts high demands on the APD.

Note that this damping measurement method, since it is based on the 1dof system equation (8), gives only reliable modal damping results if the frequencies are fully separated.

We first investigate the less critical case, i.e. the fluid damped oscillator. The center frequencies have to be set so that they lie in the appropriate attraction region and, most notably, may not have the same value during the process. We want to measure the damping of the first mode and choose $\omega_{c,1\_2} = \omega_{0,1} \pm 2\pi 100$ rad/s. The controller parameters are again adjusted using equation (30) with a time constant of $T_c = 1$ sec, the filter remains a second order Butterworth low-pass filter with 63 rad/s cut-off frequency. The phase shift difference is set to $\alpha = 45^\circ$. Figure 13(a) shows the experimental result of the simultaneous tracking of two frequencies that evolve corresponding to the targeted phase shift values. The frequencies reach the final value after approximately two seconds and hold it stably. Since the mean value of the two frequencies is the resonance frequency, the damping ratio can directly be calculated using equation (8). As shown in Figure 13(b) the damping can be determined with good accuracy, the error is only 1.4%.

As an example that poses higher demands on the frequency separation, the first mode of the lightly damped oscillator is now studied. Since the damping is very low, the frequency difference is expected to be only about 2 rad/s at $\alpha = 45^\circ$. However, the low-pass filter must be able to effectively filter out this frequency difference, cf. equation (16). Therefore, the cut-off frequency of the second order Butterworth filter has been set to 0.3 rad/s for this experiment. To avoid any overshoot of the frequencies, the time constant of the controller parameters is set to $T_c = 10$ sec and the center frequencies are $\omega_{c,1\_2} = \omega_{0,1} \pm 2\pi 2.5$ rad/s. With these rather conservative adjustments, the frequency separation was also possible for the lightly damped oscillator, as shown in Figure 14. Due to the slow filter and the chosen controller parameters the evolution is relatively slow. Furthermore, a significant oscillation in the

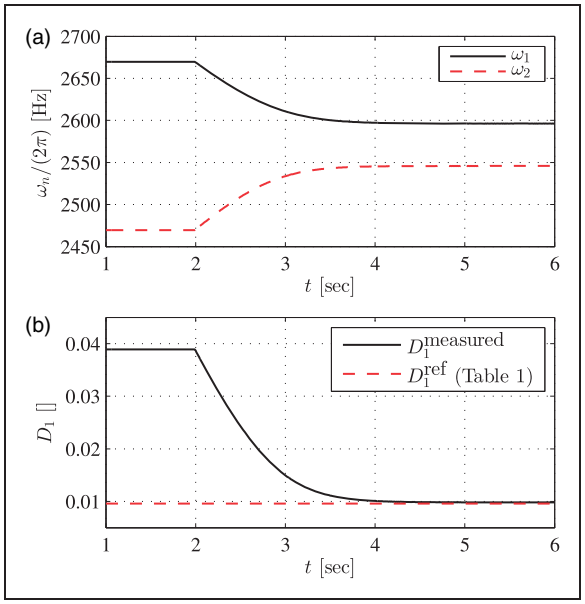

Figure 13. Experimental result of the direct damping measurement of the first torsional mode of the fluid-damped oscillator: Two PLL subsystems control two frequencies corresponding to the same vibration mode but using two different reference values $\Delta\phi_{\text{ref}} = \pm 45^{\circ}$. Cut-off frequency $\omega_{3\text{dB}} = 63$ rad/s – (a) Evolution of the excitation frequencies; (b) Measured damping ratio.

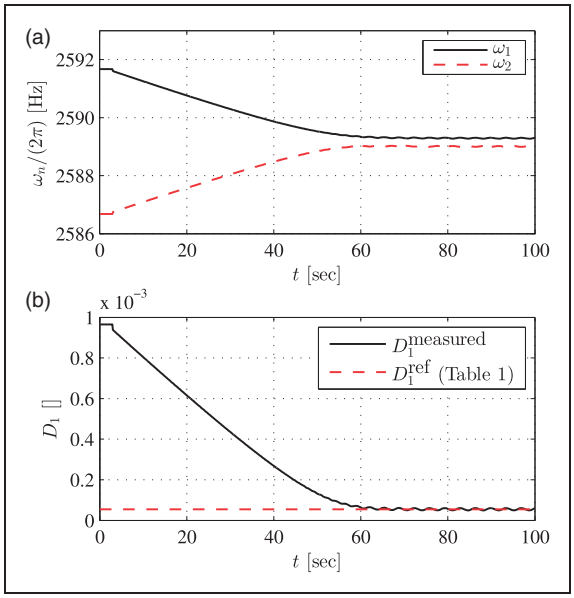

Figure 14. Experimental result of the direct damping measurement of the first torsional mode of the oscillator in air: Two PLL subsystems control two frequencies corresponding to the same vibration mode but using two different reference values $\Delta\phi_{\text{ref}} = \pm 45^{\circ}$. Cut-off frequency $\omega_{3\text{dB}} = 0.3$ rad/s – (a) Evolution of the excitation frequencies; (b) Measured damping ratio.

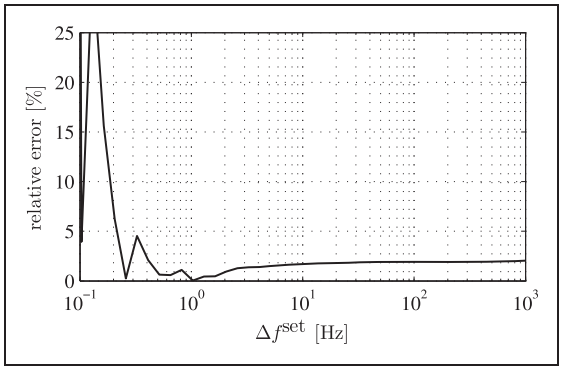

Figure 15. Relative error of the measured frequency difference with respect to the theoretical frequency difference Δf^{set} of a 1dof oscillator. The results are obtained by numerical simulations of the direct damping measurement method. The cut-off frequency of the low-pass filter is set to 1/5 of Δf^{set}, the measurement is carried out after 500 seconds.

final value can be observed. By averaging over the last five seconds, the accuracy of the calculated damping ratio is still very good, showing an error of only about 2%.

The presented results show the frequencies evolving from the center frequencies to the end value, mostly for illustration purposes. However, the start-up process is only necessary at the beginning of the measurement. Once locked in at the correct frequency, the controller parameters can be changed and variations in the damping of the system can be tracked very quickly. The minimum damping ratio that is measurable with the presented method is dependent on the effective separation of two adjacent frequencies. Therefore, a series of numerical simulations of the measurement method has been performed where the oscillating system is represented by a 1dof system with properties that are changed such that the theoretical final frequency difference at $\alpha = 45^{\circ}$ covers a range of $\Delta f^{\text{set}} = 10^{-1} \ldots 10^{3}$ Hz. In this simulation, the cut-off frequency of the filter is set to 1/5 of the expected frequency difference, the excitation frequencies are measured after 500 seconds by averaging over the last second. Figure 15 depicts the relative error of the measured frequency difference with respect to the pre-set value Δf^{set}, showing that a frequency difference greater than 2×10^{-1} Hz can be measured with an error less than 10%. As an example, this corresponds to a damping ratio of approximately 4×10^{-5} if the resonance frequency is equal to $\omega_{0,1}$. The constant error at higher frequency difference values of about 2% is due to the fixed sampling rate of the simulation.

5. Conclusions and outlook

A digital control system that is able to simultaneously control multiple frequencies of an oscillator was

presented. The combination of multiple independent phase-locked loops with the oscillator enables the simultaneous phase control of multiple frequencies. The PLLs comprise digital averaging phase detectors that combine the frequency separation and phase shift in the same element as well as simple PI controllers, which minimize the computational effort.

Using a modal separation approach, the oscillator has been modeled as a combination of several single dof systems. A linearized model of the control loop was used to investigate dynamics and stability of the control system. Based on the linear model, rules have been found to achieve the desired transient behavior for all PLL subsystems.

The investigation of the nonlinear system comprising multiple PLLs is beyond the scope of this paper and is the subject of further research.

The practical suitability was demonstrated by an experimental setup, comprising a torsional oscillator used for viscometry and a digital signal processor. By means of different surrounding media, the oscillator has been operated in two different damping conditions. The simultaneous tracking of the first five torsional resonance frequencies, as well as the direct damping measurement of the first vibration mode, have been successfully performed for both damping conditions. In particular, the direct damping measurement, which includes the discrimination of very similar (low damping) and rather diverse frequencies (high damping) illustrates the effectiveness and flexibility of the control loop. The influence of anti-resonances as boundary on the attraction of each resonance frequency has been investigated as well.

A fundamental requirement for the operation of our scheme is validity of the assumption of well separated modes. In particular, the direct damping measurement gives erroneous results if the 1dof approximation does not hold. This might be challenging if the resonance frequencies are less separated, as in the presented example. This is for instance the case when torsional and flexural modes are excited simultaneously. Specifically in the case of large damping, possible interactions have to be taken into account.

The multi-frequency control offers numerous possibilities for the improvement and enhancement of resonance-based sensor principles. Using multiple frequencies that measure the same quantity can significantly increase the accuracy of measurements. The method can also be used to distinguish between different parameters that influence the resonance frequency, e.g. to identify temperature changes of a resonator-based viscometer or to measure both viscosity and density (Ghatkesar et al., 2008). Furthermore, multi-frequency tracking enables the identification of frequency-dependent behavior, which can be used in rheometry. By receiving multiple data at once, the measurement speed of quantities that require the evaluation of multiple frequencies can be increased. This can be interesting to either monitor quickly changing processes or to increase the stability of the controlled processes.

Future work is related to practical applications of the presented method in the field of rheometry, where the evaluation of fluid properties at different frequencies is of great interest. The multi-frequency approach might also be used to evaluate the response of an oscillator excited by multiple, separate actuators, e.g. to evaluate both flexural and torsional vibrations. This can be useful to increase the sensitivity of the sensor with respect to different external influences. Further research is needed to improve the performance of the control loop in order to enable the use of even more frequencies. The development of digital control loops, with high closed-loop sample times and many parallel PLLs, is interesting but still an open challenge. Since the APD was originally designed for analog systems, alternatives might be sought that require less computational power. Such developments could make the use of low-cost microprocessors possible.

Notes

1. The term ''angular'' will be omitted throughout the rest of the paper.
2. To distinguish between time domain and Laplace domain, signals in the Laplace domain are denoted by capital letters
3. In the fluid damped situation, mode 4 has been identified by using a 2dof fit that includes the previously determined properties of mode 3.

References

Arnau A, Garcia J, Jimenez Y, et al. (2008) Improved electronic interfaces for at-cut quartz crystal microbalance sensors under variable damping and parallel capacitance conditions. *Review of Scientific Instruments* 79(7): 075110–075110–12.

Blom C and Mellema J (1984) Torsion pendula with electromagnetic drive and detection system for measuring the complex shear modulus of liquids in the frequency range 80-2500 Hz. *Rheologica Acta* 23(1): 98–105.

Brack T and Dual J (2013) Multimodal torsional vibrations for the characterization of complex fluids. *Fluid Structure Interaction VII, Wit Transactions on the Built Environment*. Vol 129WIT Press, pp. 191–200.

Brack T, Kern D, Chen M, et al. (2015) Dynamics and stability of phase controlled oscillators. *ASME Journal of Dynamic Systems, Measurement and Control* submitted.

Clarke D (2002) Designing phase-locked loops for instrumentation applications. *Measurement* 32(3): 205–227.

Dual J and O'Reilly O (1993) Resonant torsional vibrations: an application to dynamic viscometry. *Archive of Applied Mechanics* 63(7): 437–451.

Dual J, Sayir M and Goodbread J (1990) *Viscometer*. Patent 4920787, USA.

Fahy F and Gardonio P (2007) *Sound and Structural Vibration: Radiation, Transmission and Response*, 2nd ed, Academic Press.

Gardner F (2005) *Phaselock Techniques*. Wiley.

Gaspar J, Chen SF, Gordillo A, et al. (2004) Digital lock in amplifier: study, design and development with a digital signal processor. *Microprocessors and Microsystems* 28(4): 157–162.

Ghatkesar MK, Rakhmatullina E, Lang HP, et al. (2008) Multi-parameter microcantilever sensor for comprehensive characterization of newtonian fluids. *Sensors and Actuators B: Chemical* 135(1): 133–138.

Gökcek C (2003) Tracking the resonance frequency of a series rlc circuit using a phase locked loop. In: *Proceedings of 2003 IEEE conference on control applications*, pp.609–613..

Hagedorn P and DasGupta A (2007) *Vibrations and Waves in Continuous Mechanical Systems*. Wiley.

Häusler K, Reinhart W, Schaller P, et al. (1996) A newly designed oscillating viscometer for blood viscosity measurements. *Biorheology* 33(45): 397–404.

Heinisch M, Voglhuber-Brunnmaier T, Reichel E, et al. (2014) Reduced order models for resonant viscosity and mass density sensors. *Sensors and Actuators A: Physical* 220(0): 76–84.

Hsieh GC and Hung J (1996) Phase-locked loop techniques. a survey. *Industrial Electronics, IEEE Transactions on* 43(6): 609–615.

Kern D, Brack T and Seemann W (2012) Resonance tracking of continua using self-sensing actuators. *Journal of Dynamic Systems, Measurement, and Control* 134(5): 051004.

Kharrat C, Colinet E and Voda A (2008) H∞ loop shaping control for pll-based mechanical resonance tracking in nems resonant mass sensors. In: *Sensors, 2008 IEEE*, pp.1135–1138..

Kutin J, Smrečnik A and Bajsić I (2003) Phase-locking control of the coriolis meters resonance frequency based on virtual instrumentation. *Sensors and Actuators A: Physical* 104(1): 86–93.

Langdon RM (1985) Resonator sensors-a review. *Journal of Physics E: Scientific Instruments* 18(2): 103.

Oppenheim AV, Schafer RW and Buck JR (1999) *Discrete-Time Signal Processing*, 2nd ed. Upper Saddle River, NJ: Prentice-Hall, Inc.

Park S, Tan CW, Kim H, et al. (2009) Oscillation control algorithms for resonant sensors with applications to vibratory gyroscopes. *Sensors* 9(8): 5952–5967.

Rüst P, Cereghetti D and Dual J (2013) A micro-liter viscosity and density sensor for the rheological characterization of dna solutions in the kilo-hertz range. *Lab Chip* 13: 4794–4799.

Sell J, Niedermayer A and Jakoby B (2011) A digital pll circuit for resonator sensors. *Sensors and Actuators A: Physical* 172(1): 69–74.

Stokich TM, Radtke DR, White CC, et al. (1994) An instrument for precise measurement of viscoelastic properties of low viscosity dilute macromolecular solutions at frequencies from 20 to 500 kHz. *Journal of Rheology* 38(4): 1195–1210.

Sun X, Horowitz R and Komvopoulos K (2002) Stability and resolution analysis of a phase-locked loop natural frequency tracking system for mems fatigue testing. *ASME Journal of Dynamic Systems, Measurement, and Control* 124(4): 599–605.

Tjahyadi H, He F and Sammut K (2006) Multi-mode vibration control of a flexible cantilever beam using adaptive resonant control. *Smart Materials and Structures* 15(2): 270.

Vig JR (2001) Temperature-insensitive dual-mode resonant sensors – a review. *Sensors Journal, IEEE* 1(1): 62–68.

Vives A and Arnau A (2008) *Piezoelectric Transducers and Applications*. Springer.

Wang C, Yu HH, Wu M, et al. (2007) Implementation of phase-locked loop control for mems scanning mirror using dsp. *Sensors and Actuators A: Physical* 133(1): 243–249.

Wattinger T (2014) *Modeling and experimental study of a flexural vibration sensor for density measurements*. PhD Thesis, ETH Zurich, Switzerland.